



F61 Nuclear magnetic resonance

Long Report

Nils Schmitt Timo Kleinbek

Conducted in August 2018
Supervisor: Minjung, Kim

Abstract

In this experiment we started by studying the basics of magnetic excitation. In particular, we wanted to understand how exactly nuclear spins are excited to perform Larmor precession. We measured the relaxation time in the first part of the experiment. In the second part, we identified different substances by comparing the measured shifts of the Larmor frequency caused by different molecular structures. Lastly, we used nuclear magnetic resonance and different imaging methods to take pictures of several objects, analogously to the medical magnetic resonance imaging (MRI) treatment.

Contents

1. Theoretical Basics	1
2. Measurements Log and Evaluation	8
3. Critical Comment	14

1. Theoretical Basics

Basics and the relaxation time

In an applied external magnetic field, existing magnetic moments of the atomic nuclei in a material align themselves along the external magnetic field, parallel or anti-parallel. The corresponding energy splitting is given by the scalar product of magnetic moment and external magnetic field in the form

$$\Delta E = -\mu \cdot B_0. \quad (1)$$

The parallel alignment is energetically lower. The proton population numbers correctly described by the Fermi-Dirac statistics can be approximated classically by the Boltzmann distribution. The ratio of the two occupation numbers N with parallel (+) and antiparallel (-) alignment is then given by

$$\frac{N_+}{N_-} = e^{\frac{2\Delta E}{k_B T}}. \quad (2)$$

Here T describes the temperature and k_B the Boltzmann constant.

The total magnetization M results from the sum of N_+ and N_- . In general, the following applies from the electrodynamics for the resulting torque from a magnetic field and a magnetization

$$\tau = M \times B_0. \quad (3)$$

For (anti-)parallel alignment, the torque is zero. As soon as B_0 and M span a plane, the resulting torque rotates the magnetization around the axis of the magnetic field with the Larmor frequency

$$\omega_L = \gamma B_0. \quad (4)$$

Now we create a second magnetic field B_1 orthogonal to a relatively strong external magnetic field B_0 . Before the magnetization can align itself along the new total magnetic field B_{tot} , the Larmor precession around this begins. If the magnetic field B_1 oscillates with the Larmor frequency of the atomic nuclei, the magnetization can be deflected, as schematically shown in figure 1. With the

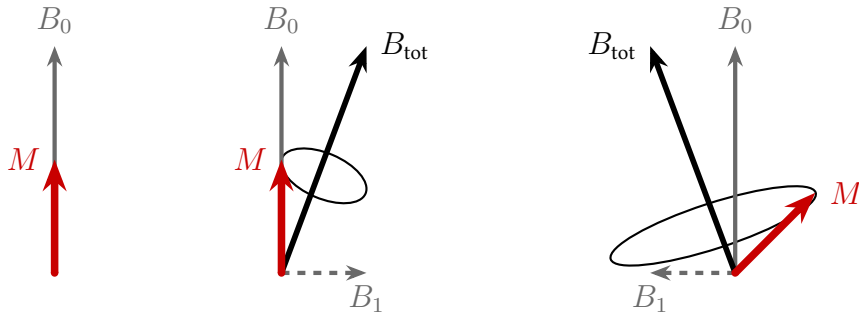


Figure 1: High-frequency external magnetic field generates elongation of magnetization.

duration of the applied high-frequency magnetic field B_1 we can determine the angle by which the magnetization is deflected compared to the external magnetic field B_0 . In particular, so-called 90° and 180° pulses can be generated, which generate an orthogonal or antiparallel magnetisation to B_0 from a parallel magnetisation.

For these excited states of magnetization, the Bloch equations describes the time development of the magentic state. The magnetization is split into a parallel and an antiparallel component in form

$$M_{\parallel}(t) = M_0 \cdot \left(1 - 2e^{-\frac{t}{T_1}} \right) \quad (5)$$

and

$$M_{\perp}(t) = M_0 \cdot e^{-\frac{t}{T_2}}. \quad (6)$$

Both change asymptotically with the characteristic time T_1 and T_2 .

The decay of the anti-parallel magnetization is caused by the interaction of the spins with the external magnetic field B_0 (spin-lattice contribution). On the other hand interactions between the individual spins (spin-spin contribution) in combination with the small spin-lattice effect lead to the decay of the orthogonal magnetization. Since the spin-spin interaction is stronger than the spin-lattice interaction, $T_2 \leq T_1$ is expected.

Measurements of orthogonal magnetization are made in the B_1 generating coil by induction. After switching off the B_1 field, the precession of the magnetization around the external magnetic field B_0 induces an alternating current in the B_1 coil. This can be measured on a connected oscilloscope. In our setup, the output signal of the induction coil leads back again into the signal generator, which generates the high-frequency alternating field B_1 , and only then into the readout devices. Thus we see the final signal as a superposition of the signal frequency and the Larmor frequency, which shows the sum and difference of the two frequencies. We also call the difference the working frequency.

The relaxation time T_1 can be measured by first passing a 180° pulse, so an antiparallel orientation of the magnetization is caused. Then after different time intervals a 90° pulse generates a signal in the induction coil whose amplitude is proportional to the magnitude of the antiparallel magnetization. By recording these amplitudes after different times, the exponential decrease of the antiparallel magnetization can be investigated and T_1 determined.

The relaxation time T_2 is measured by another combination of 90° and 180° pulses. First a 90° pulse produces a magnetization perpendicular to the B_0 field. Because of this field, the magnetization begins to precess around the B_0 axis with the Larmor frequency according to equation ???. Due to the low inhomogeneities in the magnetic field, the Larmor frequencies of the protons at different positions are different. This incoherence leads to a reduced magnetization, thus a reduced signal which is measured in the coil. After a certain time τ a 180° pulse is sent, which causes a mirroring perpendicular to the axis of the B_0 field around which the magnetization rotates. The consequence of this mirroring is that the nuclei that were in phase at $t = 0$ go back in phase at $t = 2\tau$. Because now all nuclei are in phase again, the current in the coil is maximum again.

Now you can always use different values for τ and measure the decrease of the amplitude after twice the time to reconstruct the exponential decrease. This measuring method is called spin-echo method.

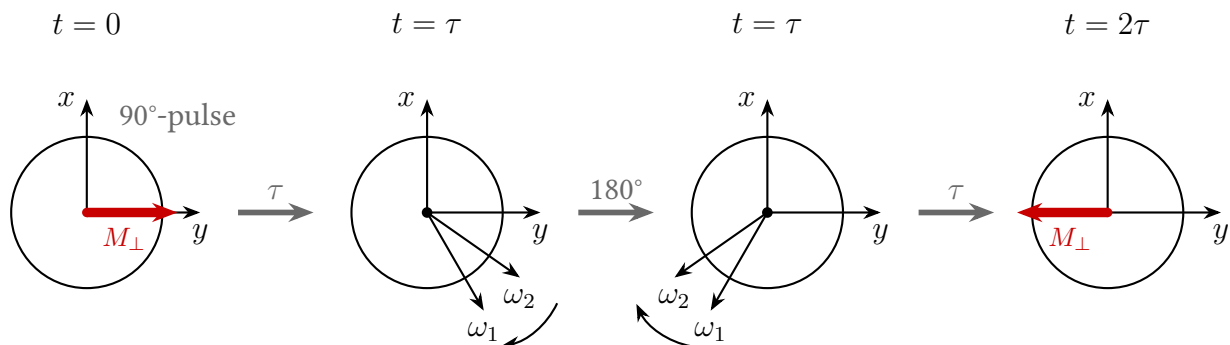


Figure 2: Diagram for measuring the relaxation time T_2 .

Alternatively, another 180° pulse can be sent to all odd multiples of time τ so that a maximum induction current is measured at all even multiples of τ . This sequence of one 90° and several 180° pulses is called the Carr-Purcell sequence. The basic procedure of the process described here is shown in figure 2 is illustrated.

Chemical Shift

When considering the excitation of nuclear spins, only atoms that actually have a nuclear spin can be excited (i. e. $S \neq 0$). Of course, a single proton as fermion in the nucleus of a hydrogen atom has a spin of $S = 1/2$. On the other hand, for a carbon atom holds $S = 0$, so there is no magnetic moment at all that could contribute to magnetization.

Additionally, note that the 90° and 180° pulses are always adjusted to a Larmor frequency. In order to achieve an effective excitation of nuclear spins of different atoms, the gyromagnetic ratio must also be the same. If we expose a sample of organic material to only one frequency that excites hydrogen nuclei, only the hydrogen atoms of an organic material will contribute to the measured Larmor frequency. In different molecules the hydrogen molecules are present in different bonds with different electronegativity differences, which means that the probability of residence of the electrons around the proton is not always the same. Due to this difference, the externally applied magnetic field B_0 is also shielded to different degrees by the electron, which results in a slightly different Larmor frequency. The magnetic field change by the electrons is described by

$$\delta\mathbf{B} = -\sigma\mathbf{B}_0, \quad (7)$$

where σ is the proportionality factor.

For a certain material, the changed Larmor frequency results accordingly from the superposition of both magnetic fields to

$$\omega_i = \omega_L(1 - \sigma_i). \quad (8)$$

In order to identify a sample on the basis of this shift of the Larmor frequency, the shielding factors relative to a reference sample Tetra-Methyl-Silane (TMS) are measured by the distance of the corresponding resonance peaks. This distance corresponds to

$$\delta_i \cdot \omega_L = \omega_{\text{TMS}} - \omega_i. \quad (9)$$

The differences of the shielding factors $\delta_i = \sigma_i - \sigma_{\text{TMS}}$ can then be looked up in a table as shown in figure 3.

The positions of the molecules in this list can be explained using the example of a COOH group.

Imaging Techniques

By excitation of nuclear spins and subsequent measurement of the magnetization, the distribution of the excited spins can be reconstructed under certain conditions and thus one-, two- or three-dimensional images of the nuclear spin distribution can be generated. To divide the material into readable pixels in the different dimensions, in addition to an external B_0 field along the z direction, we use magnetic fields, which also point in z direction but change spatially with the x , y or z coordinate. In x direction is valid for example

$$\mathbf{B}_x = (0, 0, G_x x).$$

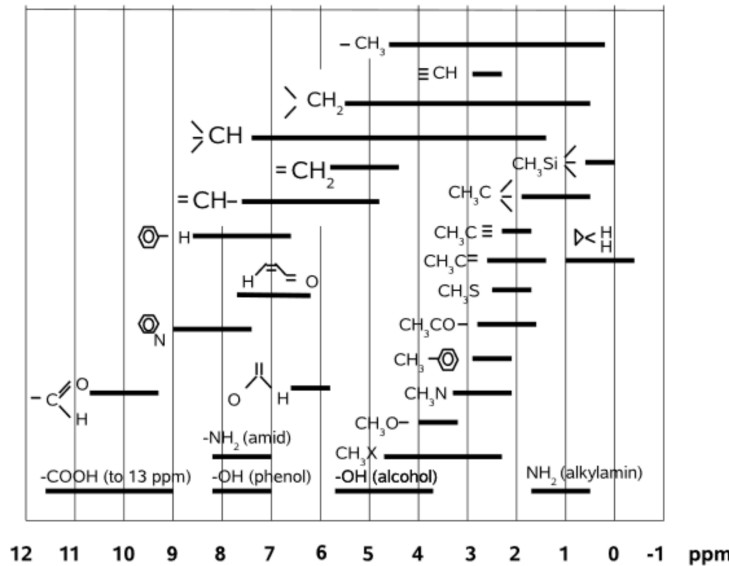


Figure 3: Chemical shifts of different molecules relative to TMS [1].

Frequency Coding

According to equation ?? the Larmor frequency in a magnetic field, which is superimposed by B_0 and a field varying in z direction, results to

$$\omega_L(z) = \gamma(B_0 + G_z z) = \omega_L^0 + \omega_z. \quad (10)$$

As soon as a 90° pulse causes a magnetization in the $x - y$ plane, this precedes the z position with different Larmor frequency around the axis of the magnetic field. The signal generated in an induction coil whose axis must be perpendicular to the z direction is then proportional to the sum of all magnetizations multiplied by the phase resulting from the high frequency ω_{HF} of the 90° pulse

$$S(t) \sim \int_V M_\perp(z, t) e^{-i\omega_{HF}t} dV, \quad (11)$$

what is equal to

$$S(t) \sim \int_V M_\perp^{\text{rot}}(z, t) e^{-i(\omega_L^0 + \omega_z - \omega_{HF})t} dV. \quad (12)$$

If we assume that $\Omega = \omega_L^0 - \omega_{HF}$, the exponential function before the integral only contributes a phase and we get

$$S(t) \sim e^{i\Omega t} \int_Z \left(\int_X \int_Y M_\perp^{\text{rot}}(z, t) dy dx \right) e^{i\omega_z t} dz. \quad (13)$$

After integration over the area of the induction coil, the measured signal is thus proportional to the Fourier transform of the magnetization. By measuring the signal at different times t_i the distribution

of the magnetization depending on the position z can be calculated by discrete Fourier transformation. As usual for functions that are linked via Fourier transform, the product of characteristic widths of the functions is constant. Therefore, the following applies

$$\Delta z \sim \frac{1}{\Delta t}. \quad (14)$$

The nuclear spins along the z coordinate have because of the inhomogeneous magnetic field different Larmor frequencies and the information of the position is “encoded” by these frequencies. Therefore we also call this method frequency coding.

For the resolution of a two-dimensional image we cannot simply use a inhomogeneous magnetic field in an additional direction because the two fields would superimpose each other and the magnetization would occur along the corresponding diagonals. Rather, we need a second type of coding, which we find in phase coding.

Phase Coding

By applying an inhomogeneous magnetic field the Larmor frequencies are different. This results in a phase difference

$$\Delta\phi(z) = \phi(z) - \phi(0) = \gamma G^z z t = \omega_z t \quad (15)$$

between the nuclear spins. If we create such a field for a fixed time T_{Ph} , the phase is dependent on the z coordinate in the form

$$\phi(z) = \gamma G^z T_{\text{Ph}} z = k_z z. \quad (16)$$

Similar to the steps above, signal and magnetization are again linked via Fourier transformation. The k_z implicitly defined above is obtained by varying the magnetic field gradient or the action time and thus receive a collection of measuring points that can be transformed back.

Two dimensional imaging

As already mentioned, we now use both of the coding possibilities mentioned to create two dimensional images. For a three-dimensional sample, we must first select a thin layer from which we want to generate the two-dimensional image. This selection is made by selective excitation of the nuclear spins in the layer to be examined. In a magnetic field gradient, for a layer whose z coordinate is between z_1 and z_2 , the Larmor frequencies are also between corresponding frequencies ω_1 and ω_2 . The transmission of a square-wave signal in the frequency space between these frequencies allows selective excitation of the desired layer. Then the nuclear spins can be encoded one after the other in the two dimensions as illustrated in figure 4.

In a first step, by applying an inhomogeneous magnetic field in x direction, different phases can be assigned to the spins in x direction, which are retained after switching off the additional inhomogeneous field, because then all spins again further precise with the same Larmor frequency.

In the last step, an inhomogeneous field is created in the y direction and the y direction is encoded in different frequencies. Here a data set is recorded directly in a certain time interval. To scroll through the pixels in the x direction, the k_z must be changed again. This produces a two-dimensional data set, which is again transformed into an image by two dimensional inverse Fourier transformation.

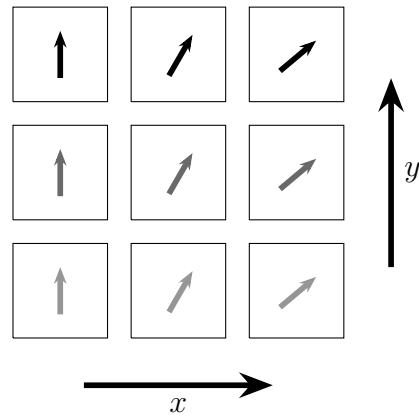


Figure 4: Spins for two-dimensional images, where the direction of the arrow symbolizes the phase and the grayscale the frequency.

The procedure of this data acquisition is shown in figure 5.

It is obvious that by stimulating individual layers and creating the respective images one after the other, three-dimensional objects can also be examined. This procedure is used extensively in medicine. For this reason, however, MRI must also ensure that the sample is completely immobilised, as temporal sequences cannot be displayed.

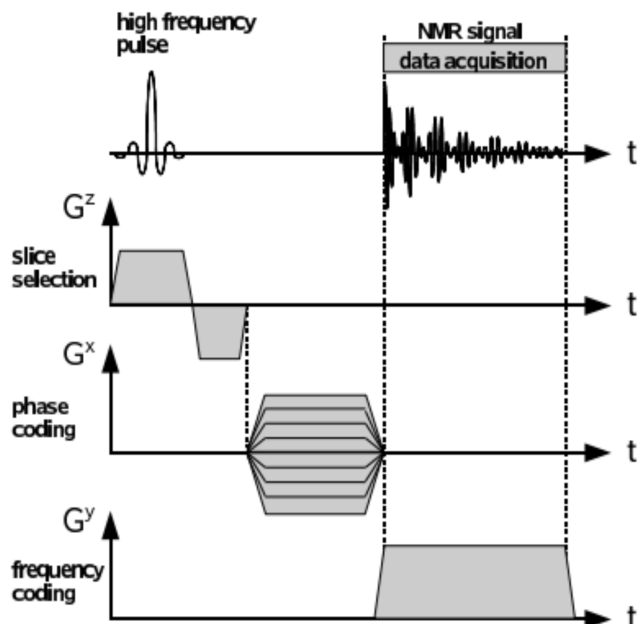


Figure 5: Data recording for two-dimensional imaging [1].

2. Measurements Log and Evaluation

Experimental setup

The relaxation times and the chemical shift were measured with a Bruker minispec p20 (see fig. 6). The arrangement is divided into the p20 electrical unit and the p20 magnet.

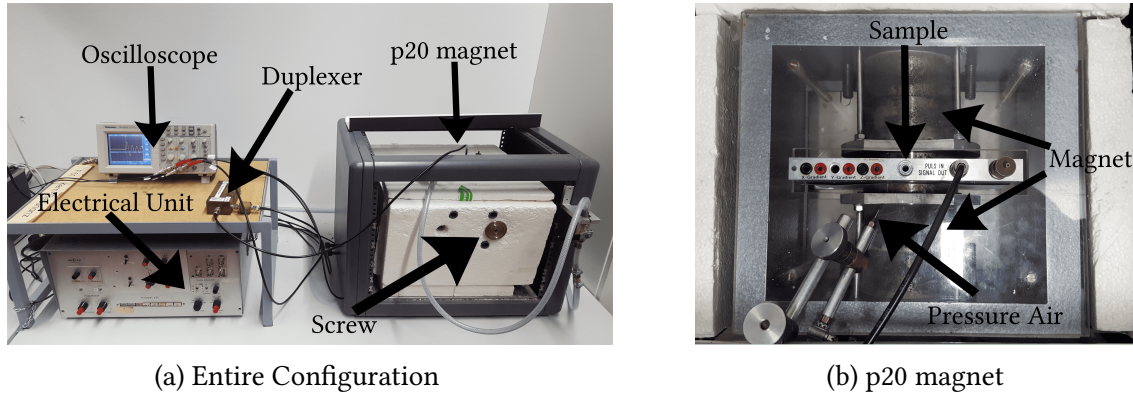


Figure 6: Experimental setup.

The electrical unit can generate two different pulses (hereinafter called pulse I and pulse II), as well as I-I, I-II and II-I sequences and a Carr-Purcell sequence. For the sequences the duration between the individual pulses and for the individual pulses the pulse duration can be set. The latter was later adjusted so that the two pulses correspond to a 90° or 180° pulse. The signal generated by the electrical unit is conducted into the magnet, where it generates a magnetic field that deflects the magnetic moments of the atomic nuclei in the sample. These rotate as described in the previous section with the Larmor frequency and generate a signal with this frequency in an induction coil inside the structure. This signal is fed back into the electronic unit via the duplexer, where it is modulated with the high-frequency excitation frequency. The resulting signal has a working frequency which indicates the difference between the excitation frequency and the Larmor frequency. This is displayed on the oscilloscope and read out and evaluated on the PC with LabView.

Determination of relaxation time

Spin-spin interaction T_2 using spin-echo method

As described in the theoretical principles, different time spans τ were set as the interval duration between the 90° pulse and the 180° pulse and the intensity of the observed echo was measured after each period of 2τ , when all spins again contributed in phase to a maximum induction current.

When measuring the Gd500 sample we regularly checked the working frequency values and found that this value increased from initially $\omega_f = (900 \pm 40)$ Hz to now $\omega_f = (1150 \pm 20)$ Hz and finally to $\omega_f = (1170 \pm 20)$ Hz. The reason for this is a change in the Larmor frequency of the hydrogen atoms due to a change in the external magnetic field B_0 , which is caused by temperature fluctuations in the laboratory. Although we tried to check the working frequency regularly and correct any deviations with the screw shown above, this inconsistency of the working frequency has effects on our measurement results that have yet to be discussed.

If echo times are too high, diffusion changes the position of the atoms so they are no longer all in phase again at the corresponding echo time. This effect reduces the intensity of the echo signal by

independent migration and change of the magnetic field.

The results of the measurement for the Gd500 sample and the equivalent Gd600 sample are plotted with Python in Figure 7 and provided with an exponential fit according to equation 6. This way we

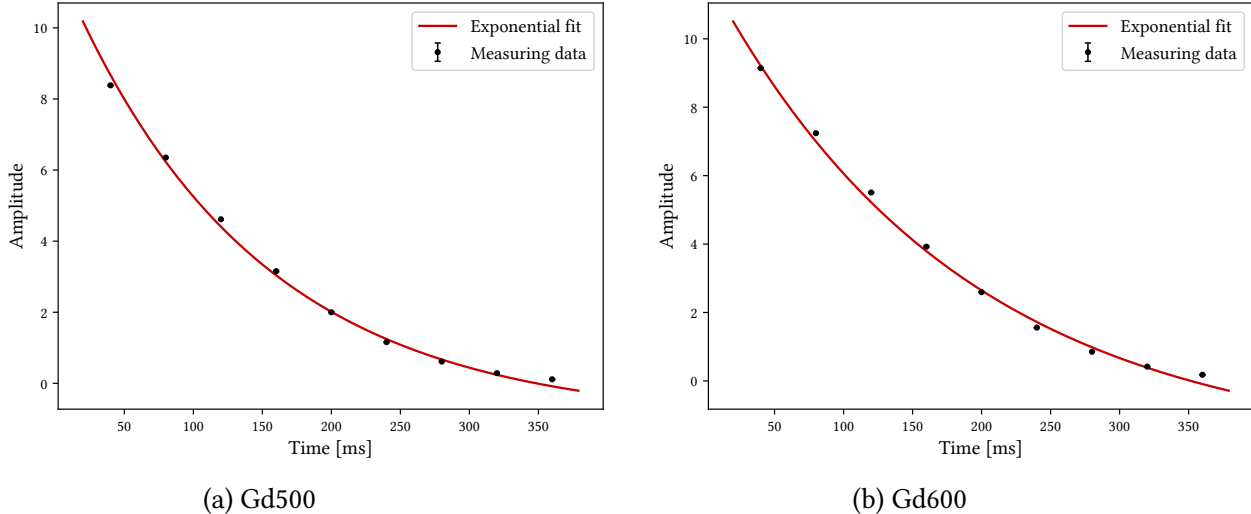


Figure 7: Results of the measurement for relaxation time T_2 using spin-echo method

get the relaxation times

$$T_{2, \text{Gd500, spin-echo}} = (154.2 \pm 0.9) \text{ ms}, \\ T_{2, \text{Gd600, spin-echo}} = (186.5 \pm 0.9) \text{ ms}$$

for our measurement.

Spin-spin interaction T_2 using Carr-Purcell method

The only difference between the Carr-Purcell method and the previous spin-echo method is the recurring 180° pulse, so that echo signals appear again and again at intervals of 2τ and the exponential decrease in amplitude can already be seen in one signal.

Because the values are recorded directly one after the other and possible inconsistencies in the magnetic field or other parts of the test setup do not have such a large influence, the results of the Carr-Purcell series of measurements appear more credible.

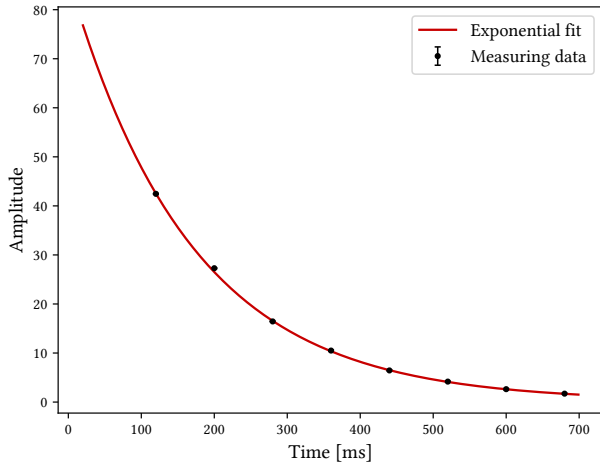
After the Python fit we get the values

$$T_{2, \text{Gd500, Carr-Purcell}} = (170.1 \pm 0.4) \text{ ms}, \\ T_{2, \text{Gd600, Carr-Purcell}} = (198.2 \pm 0.7) \text{ ms}$$

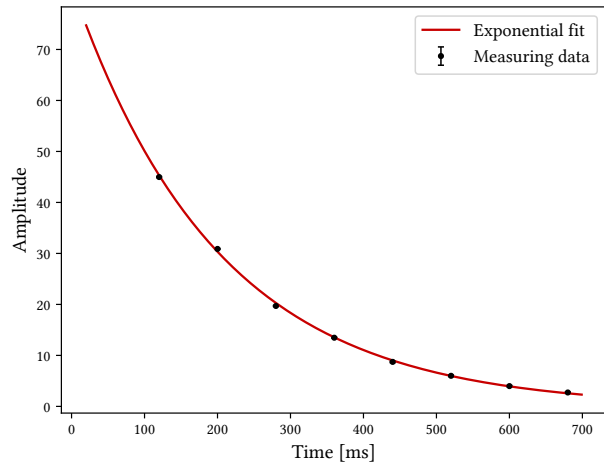
from figure 8.

Spin-lattice interaction T_1

With the sequence of 180° and 90° pulses described in the basics after different times and respective intensity measurement of the signal after this time, the increase of magnetization in the direction of



(a) Gd500

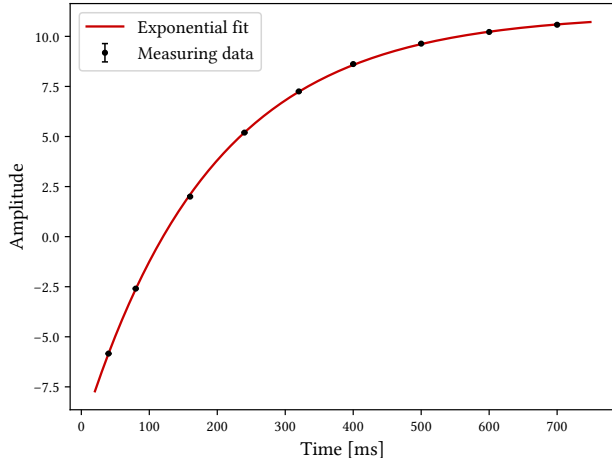


(b) Gd600

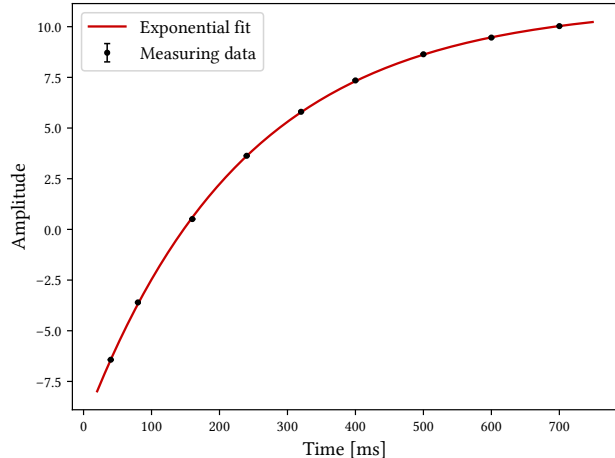
Figure 8: Results of the measurement for relaxation time T_2 using Carr-Purcell sequence.

the magnetic field can be measured.

The corresponding plots for the relaxation time of the spin-lattice interaction T_1 for both gadolinium samples are shown in figure 9. With the help of Python, an exponential fit according to equation 5



(a) Gd500



(b) Gd600

Figure 9: Results of the measurement for relaxation time T_1 .

gives the values

$$T_{1,\text{Gd500}} = (190.0 \pm 0.6) \text{ ms},$$

$$T_{1,\text{Gd600}} = (234.3 \pm 0.5) \text{ ms.}$$

Table 1 summarizes all three measured relaxation time values for both samples. We see that all relaxation times for the more diluted sample Gd600 are longer than with Gd500. This results directly from the lower Gadolinium content because Gadolinium reduces the relaxation time.

Sample	T_1 [ms]	$T_{2, \text{spin-echo}}$ [ms]	$T_{2, \text{Carr-Purcell}}$ [ms]
Gd500	190.0 ± 0.6	154.2 ± 0.9	170.1 ± 0.4
Gd600	234.3 ± 0.5	186.5 ± 0.9	198.2 ± 0.7

Table 1: Measured relaxation time.

Within the measurements of a sample we also see that the spin-echo method delivers shorter times than the Carr-Purcell method. This is due to the longer recording time of the spin-echo method, in which the sample has time for diffusion and the magnetic field can change.

The relaxation time T_2 of spin-spin interaction is less than that of spin-lattice T_1 , because the latter includes the energy release into the environment, while the spin-spin interaction only takes into account the behavior within the molecules. In general, the theoretical prediction

$$T_1 \geq T_2 \quad (17)$$

can be determined. In order to release energy into the environment, however, it requires a certain threshold value that is higher than that required to perform a spinflip in the molecules. Therefore, the time for the spin-lattice interaction is longer than for the spin-spin interaction.

Chemical shift

In this part of the experiment we measured the Larmor frequencies of unknown substances with and without the reference substance TMS. This was done by measuring the resonance peaks of the Fourier transform of the registered signal. We can measure a signal in the frequency spectrum from 200 to 900 Hz, which is determined by our magnet. If we also use pressure air to put our probe into rotation, the width of the frequency response becomes smaller. From the frequency shift measured in this way, the chemical shift can be calculated using equation 9.

Sample	Shift 1 [ppm]	Shift 2 [ppm]	Shift 3 [ppm]	Substance
A	2.4 ± 0.1	3.9 ± 0.1	6.3 ± 0.1	fluoroacetone
B	2.1 ± 0.1	6.9 ± 0.1		p-xylol
C	9.6 ± 0.1	12.0 ± 0.1		acetic acid
D	4.0 ± 0.1	6.4 ± 0.1		fluoroacetonitril
E	2.2 ± 0.1	7.3 ± 0.1		tuluol

Table 2: Measured chemical shifts.

Experimentally, we had to give a pulse to the magnet every three seconds and continuously adjust the main magnetic field so that the working frequency is around $\nu_w = 500$ Hz. Therefore, one wavelength had to be 2 ms long, which we could achieve via the screw on the magnet.

Table 2 lists the measured chemical shifts of the different samples and their assignment to the corresponding chemical elements. Due to missing samples A,D and E, the shifts could unfortunately only be taken over by leading test participants.

Now we knew that the elements toluol ($\text{CH}_3 - \text{C}_6\text{H}_5$), p-xylol ($\text{CH}_3 - \text{C}_6\text{H}_4 - \text{CH}_3$), acetic acid ($\text{CH}_3 - \text{COOH}$), fluoroacetone ($\text{FCH}_2 - \text{CO} - \text{CH}_3$) and fluoroacetonitrile ($\text{FCH}_2 - \text{CN}$) were among the samples

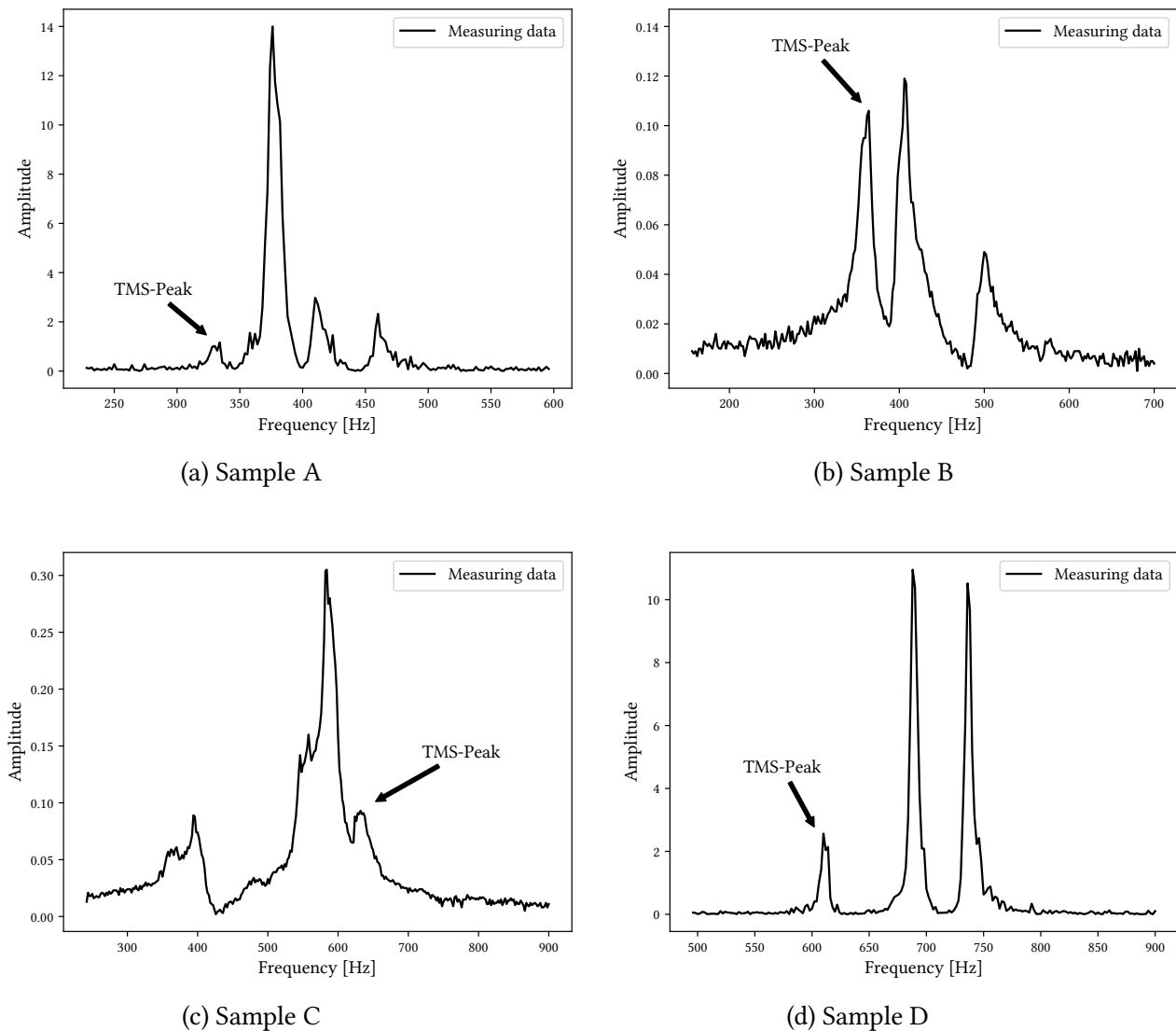


Figure 10: Fourier transform of the registered signal.

and could classify them according to the same principle with figure 3.

Sample C is the only one that has a shift above 10 ppm and therefore must have a COOH group, which only applies to acetic acid. The two shifts of samples B and E are in fact the same. The same functional groups, a carbon ring and one or two methyl groups for tuluol and p-xylol, cause the same shifts. Because p-xylol contains twice the amount of methyl groups, this substance should show a higher ratio in the peak heights. Sample B shows exactly such a difference and is therefore p-xylol, while sample E is then tuluol. Both fluoroacetone and fluoroacetonitril have a fluoromethyl group and show two identical shifts. Nevertheless, the former has a third shift exactly the same size as tuluol and p-xylol, which could be assigned to the simple methyl group. Therefore, sample A with the additional peak corresponds to fluoroacetone and sample D to fluoroacetonitril.

Imaging techniques

The following part for the one and two dimensional imaging was performed with a Bruker NMR analyzer mq7. 5 and evaluated with software provided by Bruker.

One dimensional imaging

First we examined the paintings of different heights of oil, as well as when Teflon layers are between the oil. Figure 11 shows very well the structural resolution of the NMR technology.

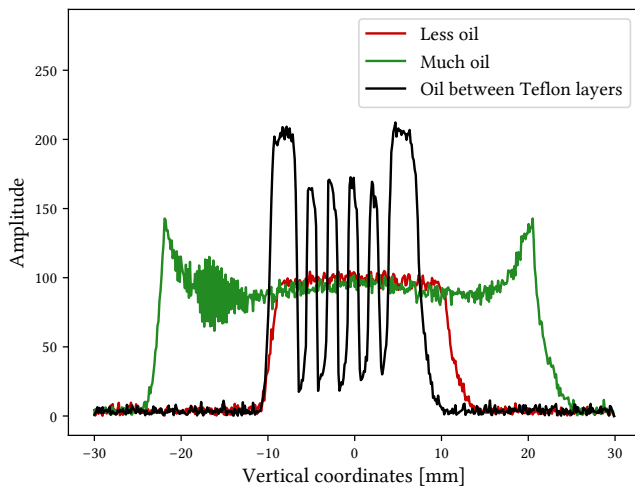


Figure 11: Various oil samples.

Since the analyzer used is calibrated for hydrogen, we expect signals proportional to the hydrogen density. For oil this corresponds to a square-wave signal, while Teflon consists of C_2F_4 units and is therefore not excited.

At first glance you can see that the red curve only has a small but constantly wide peak for the small oil content. On the other hand, the green curve for the large amount of oil at both ends is increased again because the range of the homogeneous magnetic field ends. In the black curve, the individual Teflon layers, which cannot be detected in the NMR and therefore have no amplitude, can be easily recognized again.

Furthermore, we filled a test tube up to about 2 cm with sand and poured oil over it. Now we have made regular scans to investigate the seepage process (see fig. 12).

The question of whether this is diffusion can be answered with the help of Fick's Law

$$\frac{\partial c}{\partial t} = D \frac{\partial^2 c}{\partial x^2} \quad (18)$$

where c is the concentration, t the time, D the diffusion coefficient and x the positive length.

The solution of the Fick law tells us that areas with little oil must be filled slowly with individual oil droplets. This is not the case in the figure, because the fall of the curves is usually too strong at the edges. Furthermore, a diffusion process must run in negative and positive x direction, which is clearly not the case in our experiment. It is therefore not a diffusion process. This is also easy to understand, because besides Brown's molecular movement, gravity also acts as a driving force. Diffusion has a minor role in this experiment as you can see sometimes an asymptotic decrease.

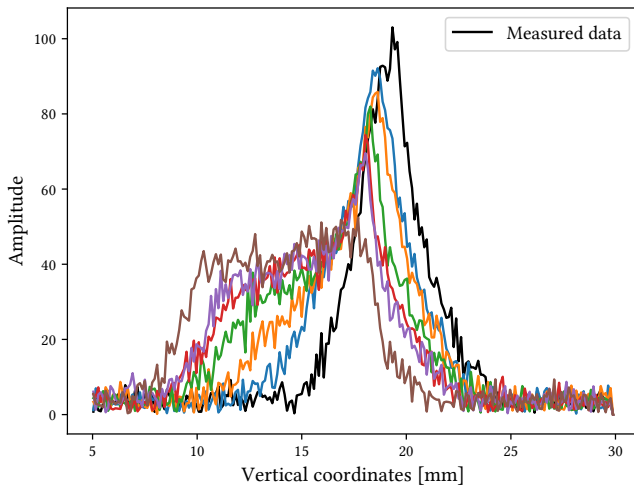


Figure 12: Seepage process of oil in sand (starts with black and ends with brown).

Two dimensional imaging

In the last part of the experiment some organic substances were analysed in the test tube, this time two dimensional cross-sections were recorded. Areas in which water is contained produce a stronger signal. So, in figure 13a we well learn, that in an olive kernel there is also a liquid. The air pockets in the peanut are also clearly visible. But we have also noticed that the correct positioning of the sample plays an enormous role and thus quickly involves a great deal of time.

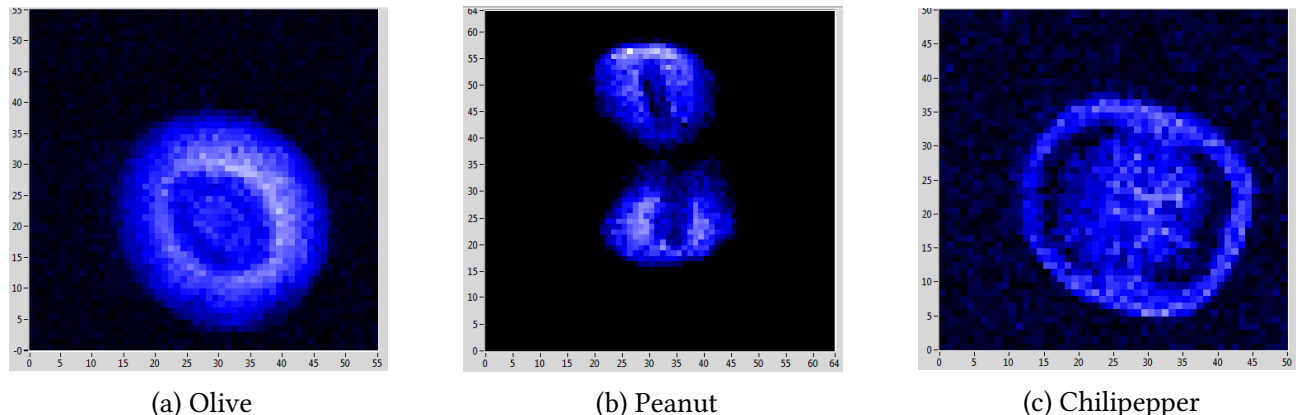


Figure 13: Two dimensional NMR imaging.

3. Critical Comment

This experiment was divided into work with a slightly older Bruker minispec p20 spectrometer and a Bruker NMR analyzer mq7.5. First of all, it can be generally said that the older device reacts very sensitively to temperature fluctuations, which is why we often had to readjust the working frequency. Nevertheless, the device was very descriptive and easily accessible from the outside, which makes it a good basis for nuclear magnetic resonance spectroscopy.

In the first part of the experiment we were able to measure the different relaxation times T_1 and T_2 of Gd500 and Gd600 with the device. We found the theoretically expected differences between the times of a sample as well as between the two samples. The times of Gd500 are smaller than those of Gd600 because Gadolinium facilitates alignment in the magnetic field. The relaxation time T_2 of spin-spin interaction is less than that of spin-lattice T_1 , because the latter includes the energy release into the environment, while the former only takes into account the behavior within the molecules. In addition, the times of the spin echo method differ from those of the Carr-Purcell method because the spin-echo method gives the sample a certain time to diffuse and the magnetic field can also change during this time.

In the second section we have determined the chemical displacement of various samples. This enabled us to assign functional groups and thus a chemical substance to each sample. The samples were rotated to compensate for inhomogeneities in the magnetic field. It is noticeable that the magnetic field is shielded differently by different groups, but the assignment by many overlaps is not so clear. This would certainly not be possible without a specification of the possible substances.

Then, using the new NMR analyzer, we used nuclear magnetic resonance spectroscopy for imaging, where the intensity of individual pixels is proportional to the water content. For example, we made one and two dimensional images of some organic and inorganic substances and examined their composition. The correct placement in the analyzer was essential, which quickly became a bit time-consuming. At the end, however, clear structures, such as the air pockets of a peanut, can be seen in the pictures.

Thus, the experiment was very good to gain insights into NMR, which is of course of great importance in medicine.

References

- [1] R. Schicker. "Nuclear Magnetic Resonance F61/F62. Manual 2.0". en. In: (Apr. 14, 2010). URL: <https://www.physi.uni-heidelberg.de/Einrichtungen/FP/anleitungen/F61.pdf>.